Lab on a Chip

Accepted Manuscript

RSC Publishing

www.rsc.org/loc

Registered Charity Number 207890

We developed a local redox cycling-based electrochemical (LRC-EC) system for the detection of a droplet array.

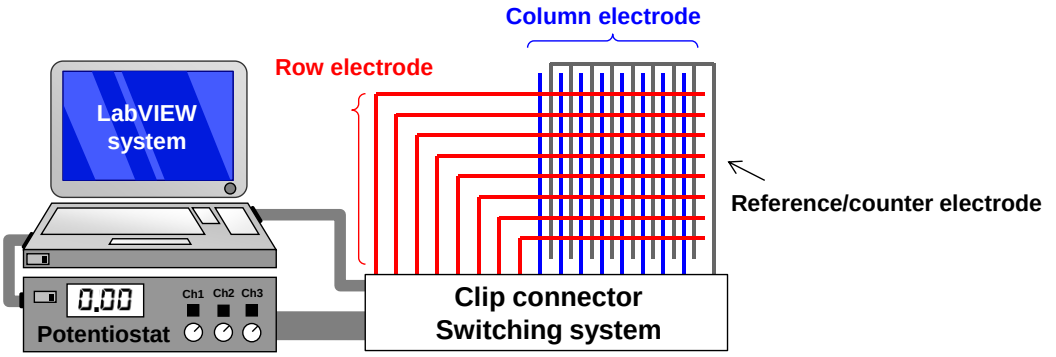

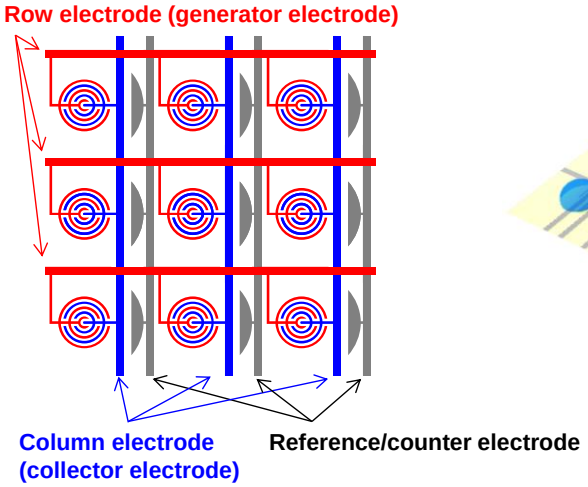

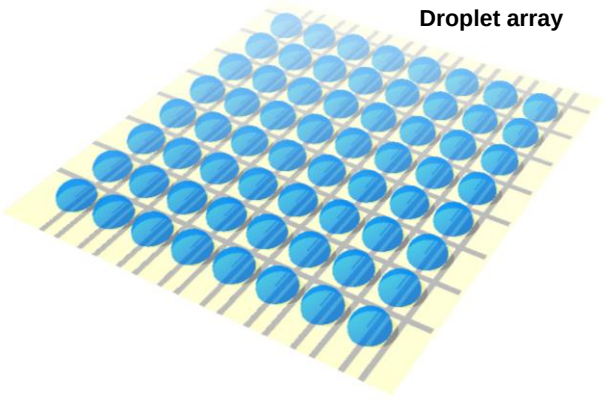

Droplet array on local redox cycling-based electrochemical (LRC-EC) chip device

Kosuke Ino[1], Takehito Goto[1], Yusuke Kanno[1], Kumi Y. Inoue[1], Yasufumi Takahashi[2], Hitoshi Shiku[1], Tomokazu Matsue[1,2]

[1] Graduate School of Environmental Studies, Tohoku University, Japan.

[2] WPI-Advanced Institute for Materials Research, Tohoku University, Japan.

Corresponding authors:

Kosuke Ino (ino.kosuke@bioinfo.che.tohoku.ac.jp)

Tomokazu Matsue (matsue@bioinfo.che.tohoku.ac.jp)

Keywords:

Electrode array

Droplet array

Electrochemical detection

Redox cycling

Chip device

Abstract

We have previously reported a local redox cycling-based electrochemical (LRC-EC) system for the incorporation of many electrochemical sensors into a small chip device. In the present study, a new type of LRC-EC chip device was fabricated for the detection of a droplet array. To detect electrochemically redox compounds in droplets, Pt pseudo-reference/counter electrodes were incorporated into the individual sensors of the LRC-EC chip device. Cyclic voltammetry for the LRC-EC chip device with internal Pt pseudo-reference electrodes indicated well-defined voltammograms based on redox cycling for the individual sensor points. The device was successfully applied to the addressable detection of alkaline phosphatase (ALP) activity of HeLa cells in single droplets on the sensor points. Therefore, the LRC-EC chip device is considered to be a useful device for the bioanalysis of droplet systems.

Introduction

Several types of amperometric microelectrode arrays have been designed, fabricated and applied to chemical and biological analysis [1-5]. However, the collection of electrochemical responses at many sensors is difficult using a simple electrode array device due to a lack of space for electrodes that include sensors, lead connections, and bond pads on a small chip device. To solve this problem, we have incorporated redox cycling [6-9] into a novel electrochemical detection system for addressable detection and designated this system as a local redox cycling-based electrochemical (LRC-EC) system [10-15]. In the LRC-EC system, two arrays of n row and n column electrodes are perpendicularly arranged to fabricate an $n \times n$ array of crossing points with $2n$ bonding pads for an external connection. When an appropriate potential is applied at these electrodes, redox cycling can be introduced at desired crossing points and the crossing points can be used as individual electrochemical sensors. Therefore, many electrochemical sensors can be easily incorporated into a small area using the LRC-EC system. We have previously applied the LRC-EC system for bio-imaging and high-throughput analysis of cell activity [10-13].

Droplet systems have been developed for high-throughput analysis and highly sensitive assays in bioapplications, because samples can be compartmentalized and reactions can proceed in individually compartmentalized microenvironments for the concentration of analytes, which enables high-throughput and highly sensitive assays [16,17]. Fluorescence and chemiluminescence detection has been used for the characterization of droplets. Noji and coworkers have reported a femtoliter droplet array for a single-molecule enzymatic assay using an optical method [18-20].

Electrochemical methods have also been applied for droplet systems [21-25], among which probe-type electrodes have been applied for the detection of redox compounds in droplets [22-24]. We have previously reported double-barrel nanoprobes that contain a carbon nanoelectrode [26], and a nanoprobe that consists of a carbon nanoelectrode and a reference electrode for the electrochemical detection of alkaline phosphatase (ALP) activity in a single droplet [21]. Although the electrochemical detection of droplets using probe electrodes is simple and highly sensitive, the throughput is low. Han et al. reported a droplet-based microfluidic device containing a single electrochemical sensor for the high-throughput electrochemical assay of droplets [27]. During detection, the droplets were sequentially produced with the microfluidics and the redox compounds were detected on the electrochemical sensor in the microfluidic channel [27]. In contrast, few electrochemical devices with an electrode

array have been reported for the detection of droplet arrays because it is difficult to incorporate many electrochemical sensors into a chip device.

In the present study, the LRC-EC system was applied for array-based droplet detection. Comb-type interdigitated ring array (IDRA) electrodes were incorporated into individual sensors. In the previous LRC-EC device [10-15], it is necessary to insert reference electrodes into each droplet for detecting a droplet array, which is time-consuming and inefficient. To solve this problem, internal Pt pseudo-reference/counter electrodes were also incorporated into individual sensors for the characterization of individual droplets. The general configuration of the system is shown in Fig. 1. Redox cycling and signal amplification proceed on the IDRA electrodes [12,28,29], so that these electrodes were incorporated into the LRC-EC system. Semicircular Pt electrodes were used as pseudo-reference/counter electrodes. Wells were fabricated at the individual sensors to trap single droplets. In the present study, the LRC-EC chip device with the internal Pt pseudo-reference/counter electrodes exhibit well-defined electrochemical characteristics based on redox cycling. Furthermore, the ALP activity of HeLa in droplets was successfully detected with the device. Thus, the chemical reaction was successfully monitored in individual droplets as compartmentalized microenvironments at individual electrochemical sensors by using the new type of LRC-EC chip device.

Materials and Methods

Device fabrication

A scheme for the device fabrication process is illustrated in Fig. 2. Briefly, the device was fabricated using a conventional lithographic technique and sputtering. Ti/Pt was sputtered onto a glass substrate (Matsunami Glass Ind., Ltd., Japan) to fabricate column electrodes, IDRA electrodes, a part of the row electrodes, and pseudo-reference/counter electrodes. The row and column electrodes were connected to each IDRA electrode of a pair, which were used as generator and collector electrodes, respectively. A SU-8 (SU-8 3005, MicroChem Co., USA; 5 μm thick) insulation layer was used to cover the sensor area, except the IDRA electrodes, the Pt pseudo-reference/counter electrodes, and the row electrodes. The SU-8 layer was also used to form inner wells around the IDRA electrodes. Ti/Pt was then sputtered on the SU-8 layers to complete the row electrodes. Thus, the row and column electrodes were three-dimensionally separated by the SU-8 insulation layer. Finally, SU-8 outer wells (SU-8 3005, 5 μm thick) were fabricated on individual crossing points to prepare the 8 × 8 well array. The outer wells were used to trap the droplets.

Experimental setup for electrochemical measurement

The connector pads of the LRC-EC chip device were connected with a clip connector (CCNL-050-37-FRC, Yokowo, Japan) that was installed to a multichannel potentiostat (HA-1010 mM4, Hokuto Denko, Japan) though a switch matrix (NI PXI-2529, National Instruments, USA) (Fig. 1) [10,14]. The potentiostat and switch matrix were controlled using a program written with LabVIEW (National Instruments). A 500 mM Tris-HCl buffer containing 2 mM $MgCl_2$ (pH 9.5) was used as a buffer for all experiments. All electrochemical measurements were performed at room temperature in a Faraday cage. Droplets were introduced onto the device with a micropipette.

Cyclic voltammetry in single and dual modes for device characterization

The electrochemical performance of the device was characterized using cyclic voltammetry in a 1.0 mM ferrocenemethanol ($FcCH_2OH$) solution. The internal semicircular Pt electrodes or an external Ag/AgCl saturated KCl electrode were used as reference electrodes. The internal semicircular Pt electrode or an external Pt plate was used as a counter electrode. These electrodes were connected with the reference electrode (RE) and counter electrode (CE) terminals of the multichannel potentiostat. For characterization of the entire device, all the row and column electrodes were connected with two working electrodes (WE1 and WE2) of the multichannel potentiostat,

respectively. Cyclic voltammograms were recorded on all the sensor points covered with the $FcCH_2OH$ solution. In single mode, the potentials of WE1 and WE2 were scanned between 0.00 and 0.50 V at 20 mV/s. In dual mode, the potential of WE1 was scanned between 0.00 and 0.50 V at 20 mV/s, while the potential of WE2 was kept constant at 0.00 V.

For characterization of a single sensor, a single row electrode and a single column electrode were connected with WE1 and WE2, respectively. A single droplet (3 μL) of the $FcCH_2OH$ solution was then introduced onto the designated sensor at the crossing points of these electrodes. In single mode, the potentials of WE1 and WE2 were scanned between 0.00 and 0.50 V. In dual mode, the potential of WE1 was scanned between 0.00 and 0.50 V at 20 mV/s, while the potential of WE2 was kept constant at 0.00 V. To prevent droplet evaporation, cotton with water was placed near the sensor area and the sensor area was covered with a plastic film.

The signal amplification (ratio of oxidation current in dual mode to that in single mode) and the collection efficiency (ratio of reduction current to oxidation current in dual mode) were calculated from the currents obtained in these cyclic voltammograms at 0.50 V.

Electrochemical imaging of droplet array containing $FcCH_2OH$

Droplets (3 μL) of the solution with or without 1.0 mM $FcCH_2OH$ were introduced onto the individual sensors. Cotton with water was placed near the device to prevent the droplet from evaporation. The procedure used to detect electrochemical responses at individual sensors is described in Fig. S1 and our previous publications [10,11,14]. Briefly, redox cycling was locally induced at the desired crossing points by application of appropriate potential at the electrodes. The potential at the electrodes was sequentially changed, which results in electrochemical signals based on local redox cycling at all the crossing points that were then detected as the signals of the individual electrochemical sensors.

Electrochemical imaging of ALP activity in HeLa cells

HeLa cells were obtained from the American Type Culture Collection (ATCC, USA). HeLa cells were cultured in RPMI-1640 medium containing 10% fetal bovine serum (FBS) and 50 μg/mL penicillin/streptomycin at 37 °C under a 5% CO_2 humidified atmosphere. HeLa cells were harvested and suspended in a 4.7 mM *p*-aminophenly phosphate (PAPP; LKT Lab, USA) solution. Droplets of cell suspension (3 μL, 1.0×10^4 cells) were then introduced onto the sensors, and the ALP activity in the HeLa cells was

electrochemically detected. A scheme for the electrochemical detection of ALP activity in HeLa cells is shown in Fig. S2. Briefly, ALP in HeLa cells converts PAPP to *p*-aminophenol (PAP) during incubation. PAP is oxidized on the IDRA electrode connected to the row electrodes (0.20 V vs. the Pt pseudo-reference electrode). The oxidation product, *p*-quinoneimine (QI), then diffuses to the IDRA electrodes connected to the column electrodes and reduced back to PAP at the IDRA electrodes connected to the column electrodes (-0.40 V vs. the Pt pseudo-reference electrode). The redox cycling-based electrochemical signals from the column electrodes were acquired to estimate the ALP activity. For addressable detection, the potential at the row and column electrodes was sequentially changed (Fig. S1). Electrochemical images were constructed using the background-corrected currents because oxygen in the solution was detected at -0.40 V vs. the Pt pseudo-reference electrode.

Results and discussion

Device fabrication

Figure 3A shows that 64 IDRA electrodes and 64 Pt pseudo-reference/counter electrodes were incorporated into the LRC-EC device with only 17 connector pads. At the crossing points, the inner (130 μm diameter, 5 μm thick) and the outer wells (2.0 mm diameter, 5 μm thick) were prepared to respectively define the electrode areas and trap the droplets. The center-to-center distance of the outer wells was 2.5 mm. The width of the electrodes and gap between the electrodes in the IDRA electrodes were 6.4 and 3.6 μm, respectively.

Large amounts of Ag^+ may be toxic to mammalian cells and inhibit growth after long time exposure [30]. This problem might become much worse if the volume of the solution is small. Therefore, a Pt electrode was used as a pseudo-reference instead of an Ag/AgCl electrode. The use of a Pt electrode as a pseudo-reference can also provide simplification of the device fabrication.

An array of 64 droplets was successfully fabricated on the LRC-EC device by dropping a solution on the sensors (Fig. 3B). We have previously reported the electrochemical imaging of single droplets during evaporation using the LRC-EC chip device with an external Ag/AgCl reference electrode and an external Pt counter electrode [11]. In the present study, evaporation of the droplets was prevented by placing cotton soaked with water near the droplets to eliminate the concentration effects on electrochemical signals and thereby simplify detection in the present system.

The distance between the IDRA electrodes and the Pt pseudo-reference/counter electrodes) was approximately 450 μm; therefore, there could be a possible influence on potential control caused by the diffusion of redox compounds produced at the IDRA electrodes to the Pt pseudo-reference/counter electrodes.

Characterization of LRC-EC chip device

Figure 4 shows cyclic voltammograms of $FcCH_2OH$ using the Ag/AgCl electrode (external reference electrode) and the Pt plate (external counter electrode). In single mode of the present study, the row and column electrodes were scanned simultaneously from 0.00 to 0.50 V and the responses were acquired from the row and column electrodes, respectively. The voltammograms indicate that the currents obtained in single mode from the row electrodes were larger than those from the column electrodes because the areas of the IDRA electrodes connected to the row electrodes were larger than those of the column electrodes. In addition, the reason why is because of the edge effect since the fingers of the IDA electrodes connected to the row electrodes were placed

outside of the other of the IDA electrodes connected to the column electrodes. The signal amplification (ratio of oxidation current in dual mode to that in single mode) and collection efficiency (ratio of reduction current to oxidation current in dual mode) were calculated to be approximately 3.5 and 74%, respectively.

Figure 5 shows cyclic voltammograms using the internal Pt pseudo-reference electrodes and the external Pt plate counter electrode. The signal amplification and collection efficiency in this case were calculated to be approximately 3.4 and 73%, respectively. The voltammograms obtained using the Pt pseudo-reference electrodes were apparently shifted by -0.1 V (Fig. 5), compared with those obtained using the Ag/AgCl reference electrode (Fig. 4), which indicates that the rest potential of the Pt electrode was +0.1 V vs. Ag/AgCl electrode under the present conditions.

Figure 6 shows cyclic voltammograms obtained with the internal Pt pseudo-reference/counter electrodes. The signal amplification and collection efficiency were found to be approximately 3.4 and 73%, respectively, which are similar to those obtained under other conditions and indicates that the Pt pseudo-reference/counter electrodes were successfully used for detection of the redox compounds. However, the shapes of the voltammograms in this case were broader (Fig. 6B) than those obtained using both the internal semicircular Pt electrodes as pseudo-reference electrodes and the external Pt plate as a counter electrode (Fig. 5). Redox compounds formed at the Pt pseudo-reference electrodes during the cyclic voltammetry may affect the potential stability of the Pt pseudo-reference electrodes. In single mode voltammetry (Fig. 6B), some reduction occurs on the Pt pseudo-reference electrodes during the positive scan to compensate the oxidation at the IDRA electrodes, which results in a shift of the voltammetric profile to the positive direction.

Figure 7 shows cyclic voltammograms for a single droplet of $FcCH_2OH$ solution using the internal Pt pseudo-reference/counter electrodes (Figs. 7A and 7B). The signal amplification and the collection efficiency determined from the voltammograms (Figs. 7C and 7D) were approximately 3.5 and 75%, respectively. The shapes of the cyclic voltammograms for the single droplet were similar to those for the solution (Figs. 6B and 6C). In dual mode, the currents at 0.5 V from the row and column electrodes were 44 and -33 nA, respectively (Fig. 7D), which were 1/64 of that observed for the bulk solution (Fig. 6C). This indicates that quantitative characterization of a single droplet (3 μL) based on redox cycling is possible in a similar manner to measurement of the bulk solution. In droplet detection, the electrochemical signals at the sensor were proportional to the concentration of $FcCH_2OH$ (Fig. S3). Therefore, the LRC-EC device can be used for quantitative detection of redox components in droplets.

Electrochemical imaging of a droplet array containing $FcCH_2OH$

Figure 8 shows optical and electrochemical images of the droplet array containing $FcCH_2OH$. The electrochemical image follows the position of the droplets containing $FcCH_2OH$ on the device, and no current was acquired from a droplet without $FcCH_2OH$ (Figs. 8A and 8B). As a demonstration, the electrochemical image of a letter "E" was acquired when the droplets containing $FcCH_2OH$ were placed in an "E" configuration (Figs. 8C and 8D). These results show that addressable detection of droplets containing $FcCH_2OH$ was achieved using the LRC-EC chip device.

Although the cotton with water was applied near the sensor area and the sensor area was covered with the plastic film to avoid evaporation of the droplets, it might be necessary to use an incubator to control the humidity and temperature precisely.

Electrochemical imaging of ALP activity of HeLa cells in droplet array

Figure 9 shows time-course electrochemical images for ALP activity in HeLa cells. Droplets containing HeLa cells, PAPP, or HeLa cells and PAPP were placed on the LRC-EC chip device (Fig. 9A). Only the droplet with HeLa cells and PAPP exhibited an electrochemical signal, which indicates that the catalytic hydrolysis of PAPP to yield PAP yields electrochemical responses based on redox cycling. The electrochemical signals gradually increased during incubation as PAP was accumulated (Fig. 9) These results show that that the device can be applied for accumulation and detection of electrochemical signals from cells.

Conclusion

In the present study, an LRC-EC chip device for a droplet array was developed. Pt pseudo-reference/counter electrodes were incorporated into the individual sensors of the LRC-EC chip device to detect the droplet array. The Pt pseudo-reference electrodes on the LRC-EC chip device provided well-defined voltammetric data and signal amplification based on redox cycling. The LRC-EC chip device with the pseudo-reference electrodes was successfully applied for the detection of a droplet array. As a demonstration, the ALP activity in HeLa cells within single droplets was successfully detected. We considered that the LRC-EC chip device is useful for bioanalysis using droplet systems.

Acknowledgement

This work was supported in part by a Grant-in-Aid for Scientific Research (A) (No. 25248032) and a Grant-in-Aid for Young Scientists (B) (No. 23760745) from the Japan Society for the Promotion of Science (JSPS). This research was partly supported by Special Coordination Funds for Promoting Science and Technology, Creation of Innovation Centers for Advanced Interdisciplinary Research Areas Program from the Japan Science and Technology Agency (JST).

References

1. Kasai, N., Han, C.X. & Torimitsu, K. Hydrogen peroxide distribution and neuronal cell death in a rat hippocampal slice. *Sens. Actuator B-Chem.* **108**,746–750 (2005).
2. Cheung, K.C., Renaud, P., Tanila, H. & Djupsund, K. Flexible polyimide microelectrode array for in vivo recordings and current source density analysis. *Biosens. Bioelectron.* **22**, 1783-1790 (2007).
3. Xu, X., Zhang, S., Chen H. & Kong J. Integration of electrochemistry in micro-total analysis systems for biochemical assays: recent developments. *Talanta*, **80**, 8-18 (2009).
4. Dill, K., Montgomery, D.D., Ghindilis, A.L., Schwarzkopf, K.R., Ragsdale, S.R. & Oleinikov, A.V. Immunoassays based on electrochemical detection using microelectrode arrays. *Biosens. Bioelectron.* **20**, 736-742 (2004).
5. Pei, J.H., Tercier-Waeber, M.L., Buffle, J., Fiaccabrino, G.C. & Koudelka-Hep M. Individually addressable gel-integrated voltammetric microelectrode array for high-resolution measurement of concentration profiles at interfaces. *Anal. Chem.* **73**, 2273-2281 (2001).
6. Niwa, O., Xu, Y., Halsall, H.B. & Heineman, W.R. Small-volume voltammetric detection of 4-aminophenol with interdigitated array electrodes and its application to electrochemical enzyme immunoassay. *Anal. Chem.*, **65**, 1559-1563 (1993).
7. Kätelhön, E. & Wolfrum, B. On-chip redox cycling techniques for electrochemical detection. Rev. *Anal. Chem.*, **31**, 7-14 (2012).
8. Heo, J.I., Lim, Y., & Shin, H. The effect of channel height and electrode aspect ratio on redox cycling at carbon interdigitated array nanoelectrodes confined in a microchannel. *Analyst*, in press.
9. Rassaei, L., Singh, P.S., & Lemay, S.G. Lithography-based nanoelectrochemistry. *Anal. Chem.* **83**, 3974-3980 (2011).
10. Ino, K., Nishijo, T., Arai, T., Kanno, Y., Takahashi, Y., Shiku, H. & Matsue, T. Local redox cycling-based electrochemical chip device with deep microwells for evaluation of embryoid bodies. *Angew. Chem. Int. Ed.* **51**, 6648-6652 (2012).
11. Ino, K., Kanno, Y., Nishijo, T., Goto, T., Arai, T., Takahashi, Y., Shiku, H. & Matsue, T. Electrochemical detection for dynamic analyses of a redox component in droplets using a local redox cycling-based electrochemical (LRC-EC) chip device. *Chem. Commun.* **48**, 8505-8507 (2012).
12. Ino, K., Nishijo, T., Kanno, Y., Ozawa, F., Arai, T., Takahashi, Y., Shiku, H. & Matsue, T. Electrochemical device with interdigitated ring array electrodes for investigating the relationship between cardiomyocyte differentiation from

embryonic stem cells and alkaline phosphatase activity. *Electrochemistry* **81**, 682-687 (2013).

13. Şen, M., Ino, K., Shiku, H. & Matsue, H. Accumulation and detection of secreted proteins from single cells for reporter gene assays using a local redox cycling-based electrochemical (LRC-EC) chip device. *Lab Chip* **12**, 4328-4335 (2012).
14. Ino, K., Saito, W., Koide, M., Umemura, T., Shiku, H. & Matsue, T. Addressable electrode array device with IDA electrodes for high-throughput detection. *Lab Chip* **11**, 385-388 (2011).
15. Lin, Z., Takahashi, Y., Kitagawa, Y., Umemura, T., Shiku, H. & Matsue, T. An addressable microelectrode array for electrochemical detection. *Anal. Chem.*, **80**, 6830-6833 (2008).
16. Haeberle, S. & Zengerle, R. Microfluidic platforms for lab-on-a-chip applications. *Lab Chip*, **7**, 1094-1110 (2007).
17. Okochi, M., Tsuchiya, H., Kumazawa, F., Shikida, M. & Honda, H. Droplet-based gene expression analysis using a device with magnetic force-based-droplet-handling system. *J. Biosci. Bioeng.*, **109**, 193-197 (2010).
18. Iino, R., Hayama, K., Amezawa, H., Sakakihara, S., Kim, S.H., Matsumono, Y., Nishino, K., Yamaguchi, A. & Noji, H. A single-cell drug efflux assay in bacteria by using a directly accessible femtoliter droplet array. *Lab Chip*. **12**, 3923-3929 (2012).
19. Sakakihara, S., Araki, S., Iino, R. & Noji, H. A single-molecule enzymatic assay in a directly accessible femtoliter droplet array. *Lab Chip*. **10**, 3355-3362 (2010).
20. Kim, S.H., Iwai, S., Araki, S., Sakakihara, S., Iino, R. & Noji H. Large-scale femtoliter droplet array for digital counting of single biomolecules. *Lab Chip*. **12**, 4986-4991 (2012).
21. Ino, K., Ono, K., Arai, T., Takahashi, Y., Shiku, H. & Matsue, T. Carbon-Ag/AgCl probes for detection of cell activity in droplets. *Anal. Chem.*, **85**, 3832-3835 (2013).
22. Spaine, T.W. & Baur, J.E. A positionable microcell for electrochemistry and scanning electrochemical microscopy in subnanoliter volumes. *Anal. Chem.*, **73**, 930-938 (2001).
23. Gao, N., Zhao, M., Zhang, X. & Jin, W. Measurement of enzyme activity in single cells by voltammetry using a microcell with a positionable dual electrode. Anal. Chem., **78**, 231-238 (2006).
24. Lindsay, S., Vázquez, T., Egatz-Gómez, A., Loyprasert, S., Garcia, A.A. & Wang J. Discrete microfluidics with electrochemical detection. *Analyst*, **132**, 412-416 (2007).
25. Zhang, Y., Kim, H.H., Mano, N., Dequaire, M. & Heller, A. Simple enzyme-amplified amperometric detection of a 38-base oligonucleotide at 20 pmol L^{-1} concentration in

a 30-μL droplet. *Anal. Bioanal. Chem.*, 374, 1050-1055 (2002).

26. Takahashi, Y., Shevchuk, A.I., Novak, P., Zhang, Y., Ebejer, N., Macpherson, J.V., Unwin, P.R., Pollard, A.J., Roy, D., Clifford, C.A., Shiku, H., Matsue, T., Klenerman, D. & Korchev, Y.E. Multifunctional nanoprobes for nanoscale chemical imaging and localized chemical delivery at surfaces and interfaces. *Angew. Chem. Int. Ed.*, **50**, 9638-9642 (2011).
27. Han, Z., Li, W., Huang, Y. & Zheng, B. Measuring rapid enzymatic kinetics by electrochemical method in droplet-based microfluidic devices with pneumatic valves. *Anal. Chem.*, **81**, 5840-5845 (2009).
28. Niwa, O. & Morita, M. Carbon film-based interdigitated ring array electrodes as detectors in radial flow cells. *Anal. Chem.*, **68**, 355-359 (1996).
29. Liu, Z., Niwa, O., Kurita, R. & Horiuchi, T. Carbon film-based interdigitated array microelectrode used in capillary electrophoresis with electrochemical detection. *Anal. Chem.*, **72**, 1315-1321 (2000).
30. Li, X., & Bard A. Scanning electrochemical microscopy of HeLa cells – Effects of ferrocene methanol and silver ion. *J. Electroanal. Chem.*, **628**, 35-42 (2009).

Figure 1

General configuration of the LRC-EC system. (A) The LRC-EC chip device consists of row electrodes, column electrodes, and internal Pt pseudo-reference electrodes as generator, collector, and pseudo-reference/counter electrodes, respectively. (B) Schematic diagram of the crossing points of the row and column electrodes where the IDRA electrodes are placed. The IDRA electrodes are connected with the row and column electrodes (the IDRA electrodes are represented larger than actual for clarity). (C) Wells are fabricated to accommodate the droplet array at the crossing points.

Figure 2

Schematic illustration of the device fabrication process. (A) All column electrodes, part of the row electrodes, and all Pt pseudo-reference electrodes were fabricated on the glass substrate. The row and column electrodes were connected with the IDRA electrodes. (B) SU-8 insulation layer fabricated to form inner wells. (C) The row electrodes were then completed with three-dimensional (3D) connections. (D) Finally, the outer wells were fabricated on individual crossing points with the SU-8 layer. The ring electrodes are represented larger than actual for clarity.

Figure 3

Images of the LRC-EC chip device with internal Pt pseudo-reference/counter electrodes. (A) Optical image of the device. (B) Droplets (3 μL) are trapped on the individual sensors to form the droplet array.

Figure 4

Cyclic voltammograms for 1.0 mM $FcCH_2OH$ measured using the external Ag/AgCl electrode. (A) Schematic illustration of the electrode connections to the potentiostat. All sensors were covered with the $FcCH_2OH$ solution, and cyclic voltammetry was performed in (B) single and (C) dual modes at a scan rate of 20 mV/s.

Figure 5

Cyclic voltammograms for 1.0 mM $FcCH_2OH$ using the internal Pt pseudo-reference electrodes and the external Pt plate. (A) Schematic illustration of the electrode connections to the potentiostat. All sensors were covered with the $FcCH_2OH$ solution, and cyclic voltammetry was performed in (B) single and (C) dual modes at a scan rate of 20 mV/s.

Figure 6

Cyclic voltammograms for 1.0 mM $FcCH_2OH$ using the internal Pt electrodes as pseudo-reference/counter electrodes. (A) Schematic illustration of the electrode connections to the potentiostat. All sensors were covered with the $FcCH_2OH$ solution, and cyclic voltammetry was performed in (B) single and (C) dual modes at a scan rate of 20 mV/s.

Figure 7

Cyclic voltammograms for 1.0 mM $FcCH_2OH$ in a single droplet using the internal Pt electrodes as pseudo-reference/counter electrodes. (A) Schematic illustration of the electrode connections to the potentiostat. (B) A droplet (3 μL) was introduced to a sensor at a crossing point, and cyclic voltammetry was then performed in (C) single and (D) dual modes at a scan rate of 20 mV/s.

Figure 8

(A) Optical and (B) electrochemical images of the droplet array. Droplets (3 μL) containing 0 or 1 mM $FcCH_2OH$ were introduced onto the individual sensors and electrochemical imaging was performed. Droplets (3 μL) containing 1 mM $FcCH_2OH$ were introduced onto individual sensors in an "E" configuration and electrochemical imaging was performed (C: optical image, D: electrochemical image). These images were acquired within 30.6 s.

Figure 9

(A) Optical image of droplets including HeLa cells, HeLa cells and PAPP, or PAPP. (B) Electrochemical images obtained 10, 30, and 50 min after introduction of the droplets. The potentials of the row and the column electrodes were -0.40 and 0.20 V vs. the Pt pseudo-reference electrode, respectively.

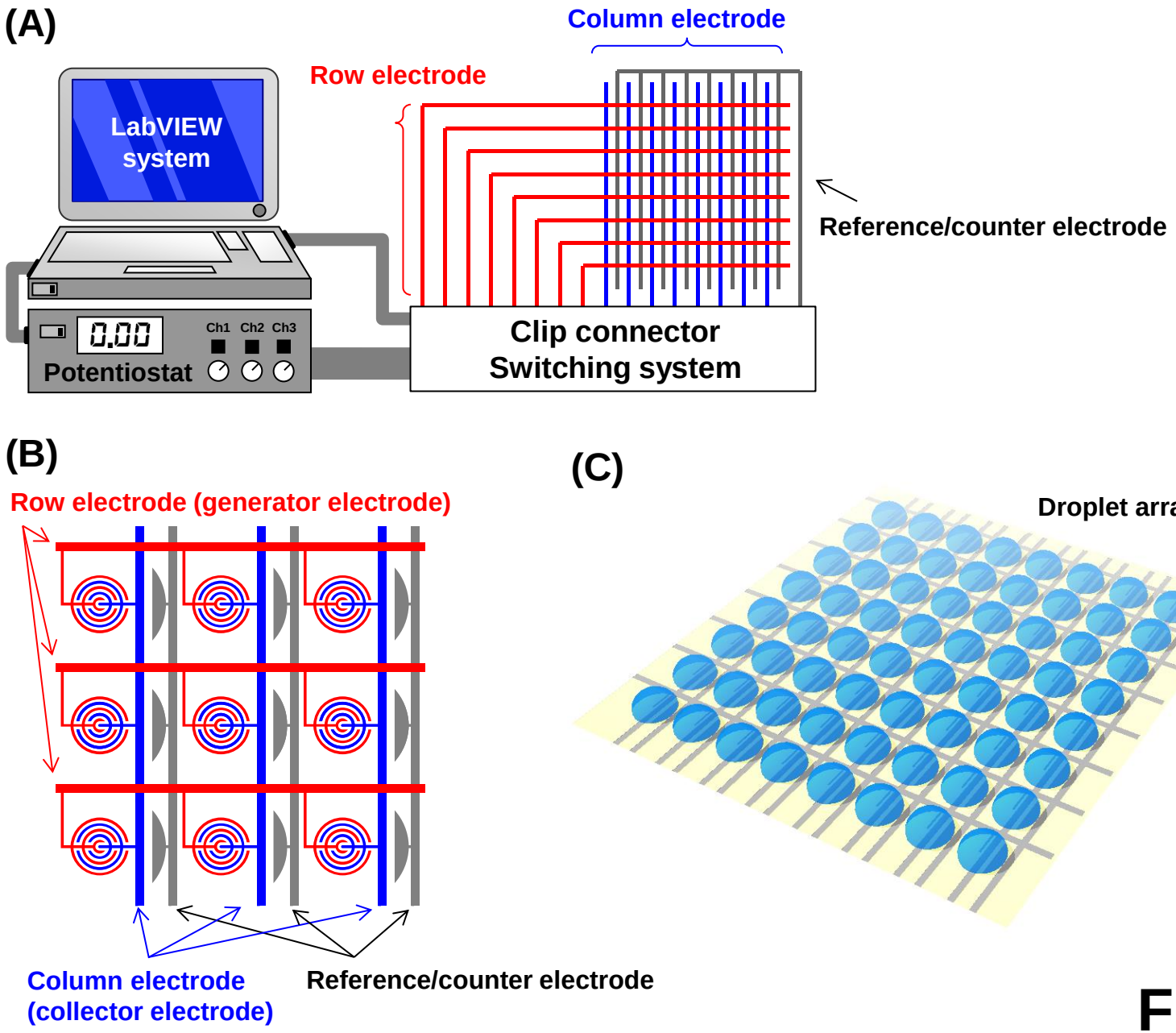

Figure 1

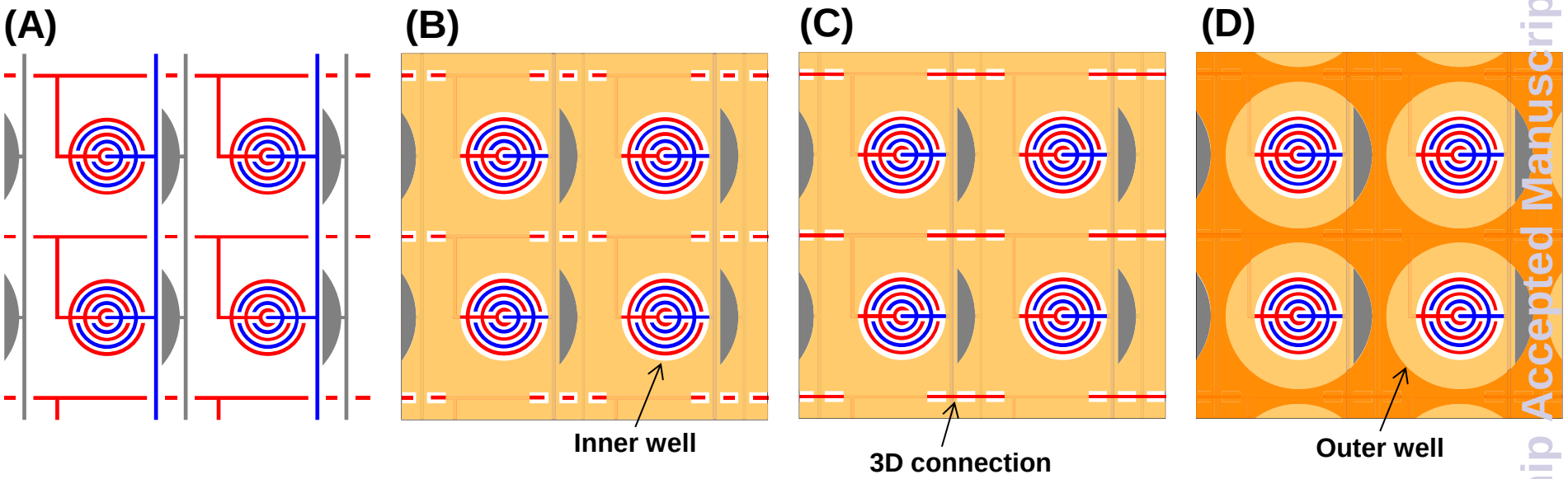

Blue: column electrode (collector electrode)
Red: row electrode (generator electrode)
Gray: reference/counter electrode
Orange: 1st SU-8 layer
Brown: 2nd SU-8 layer

Figure 2

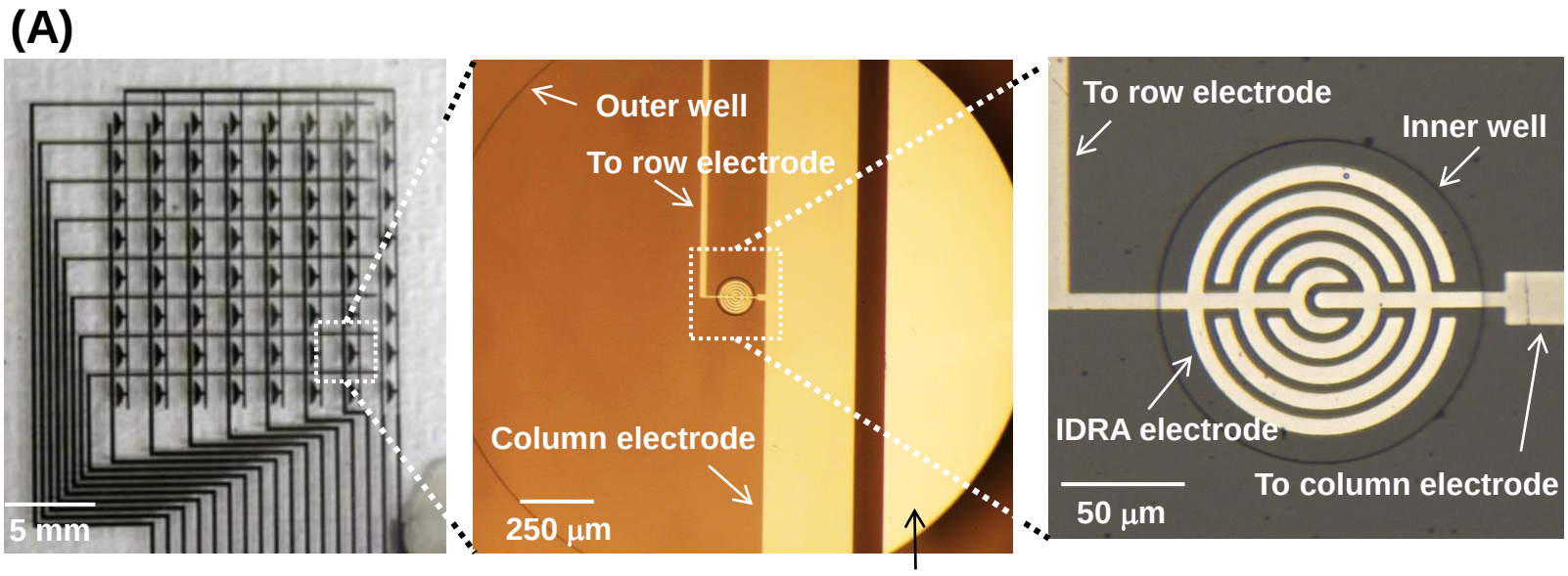

Figure 3

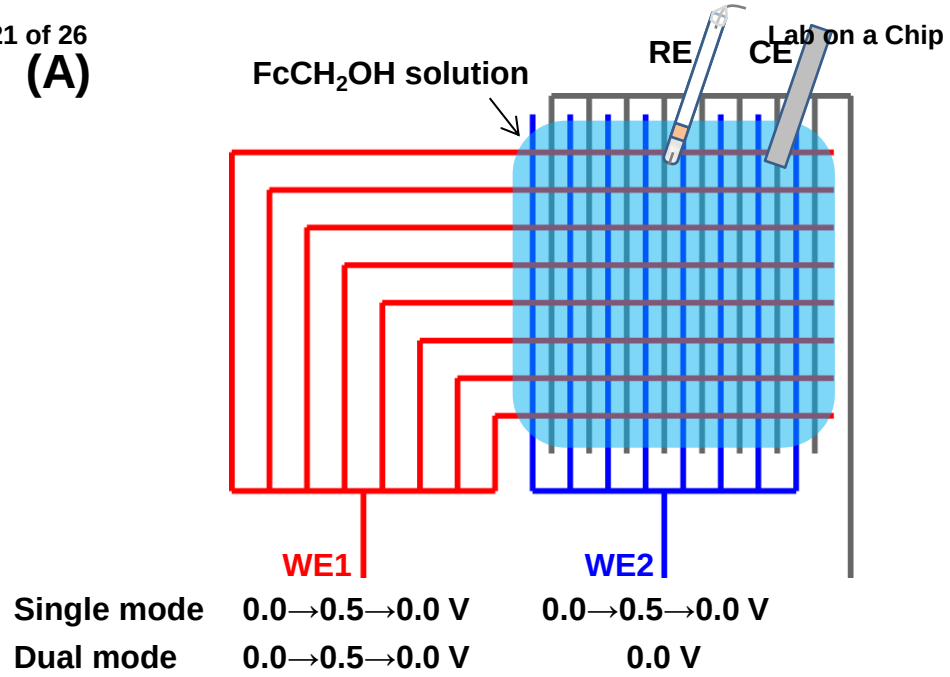

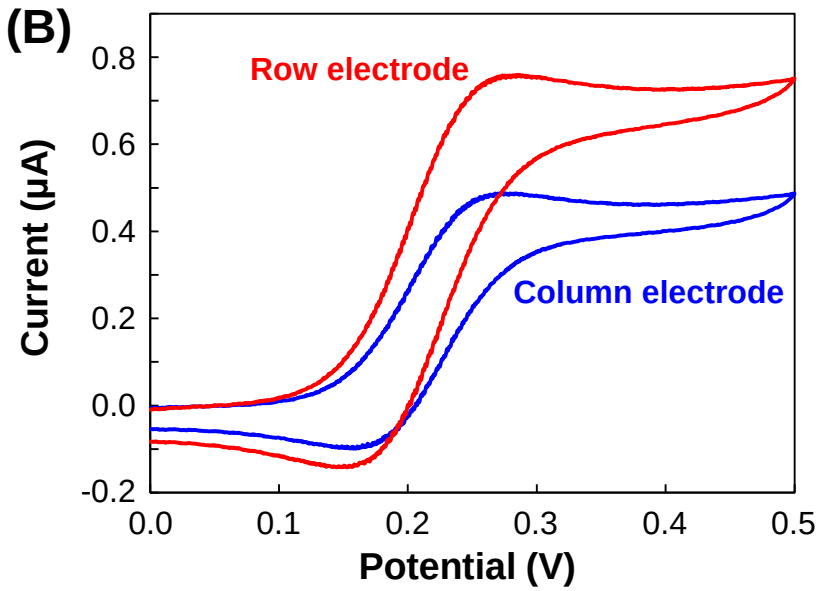

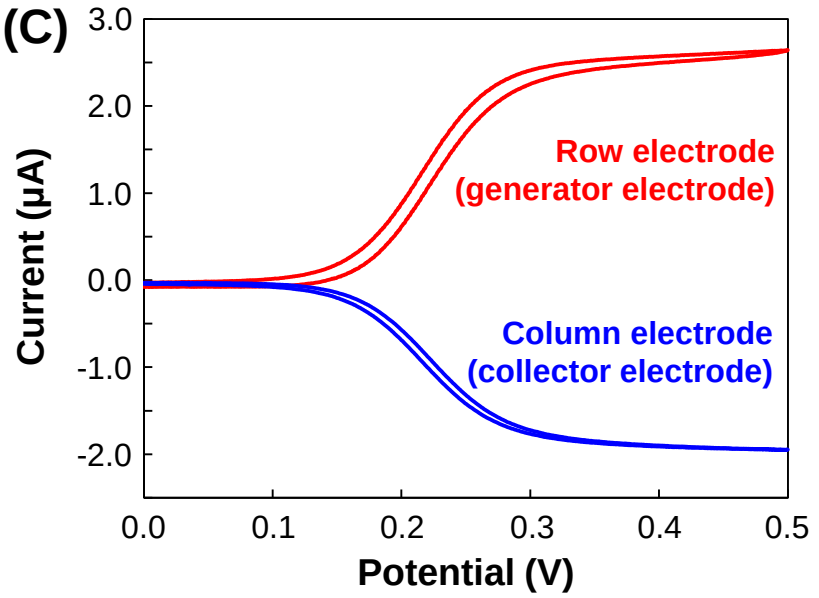

Figure 4

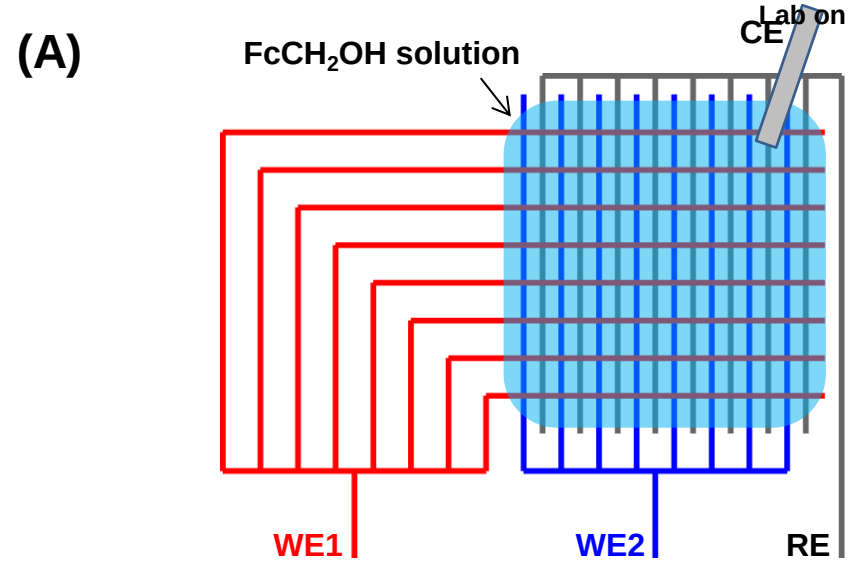

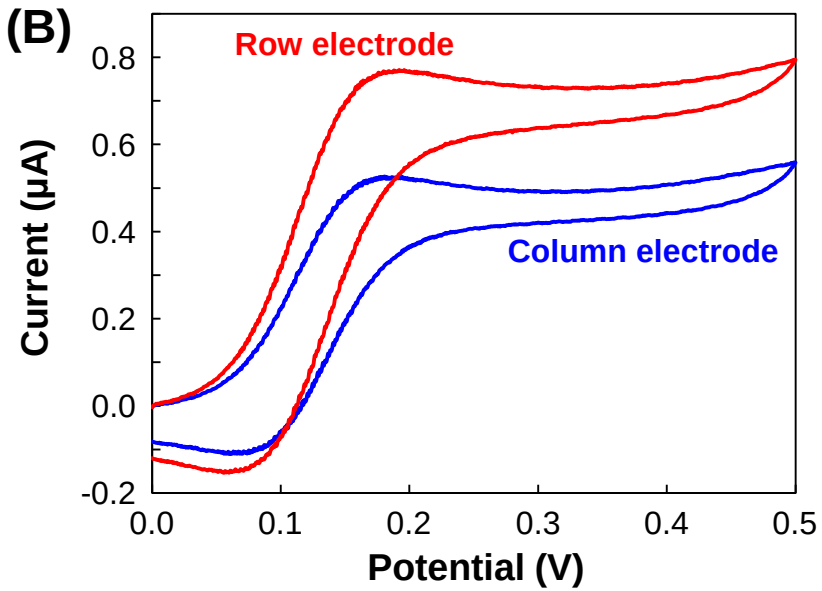

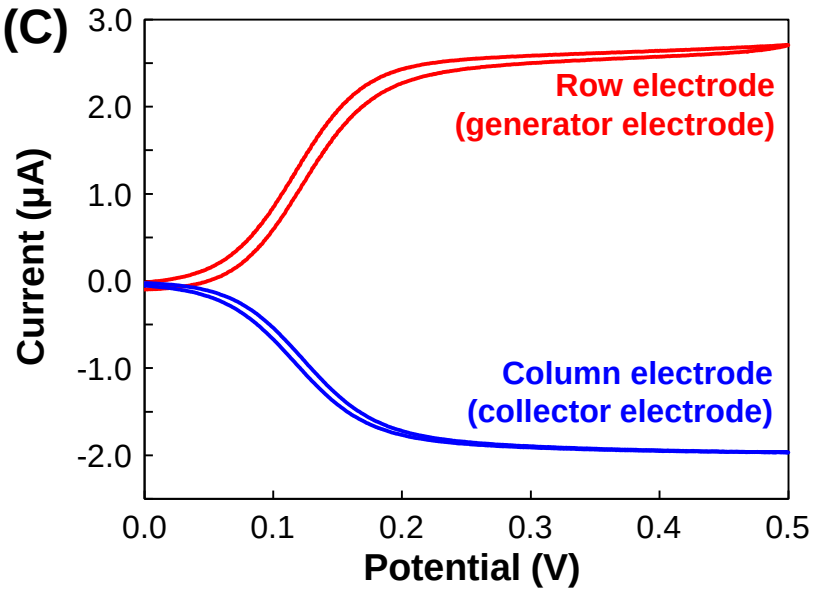

Figure 5

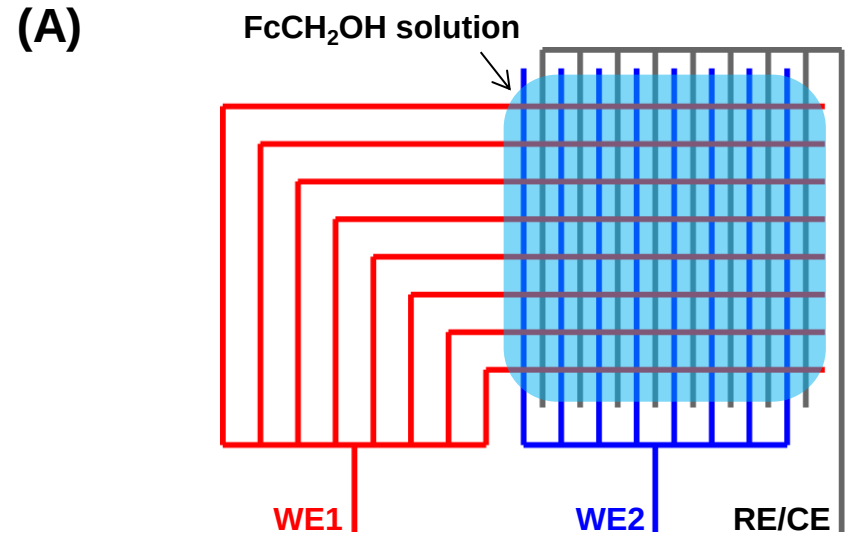

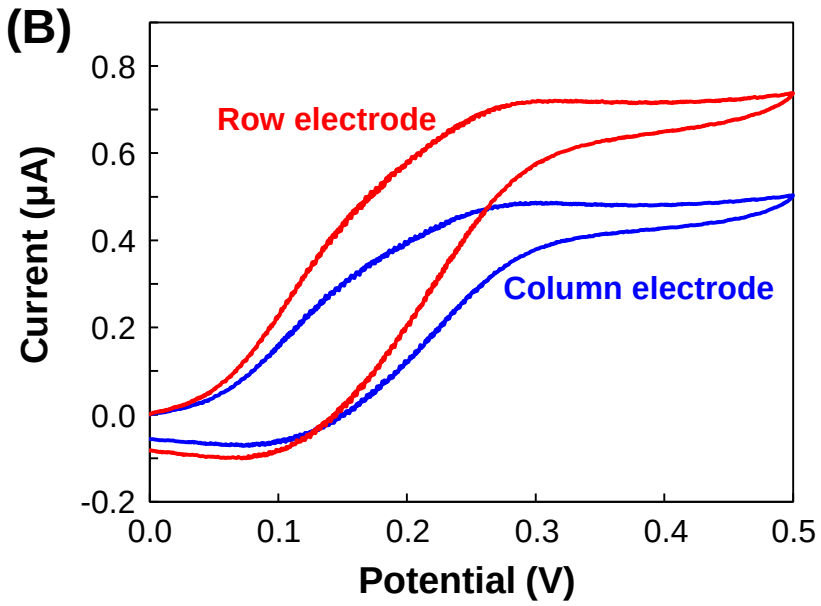

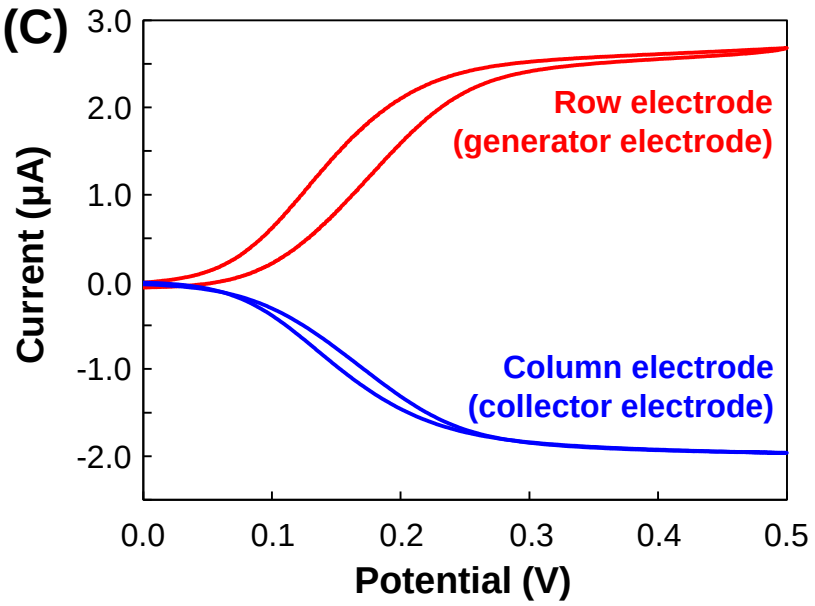

Figure 6

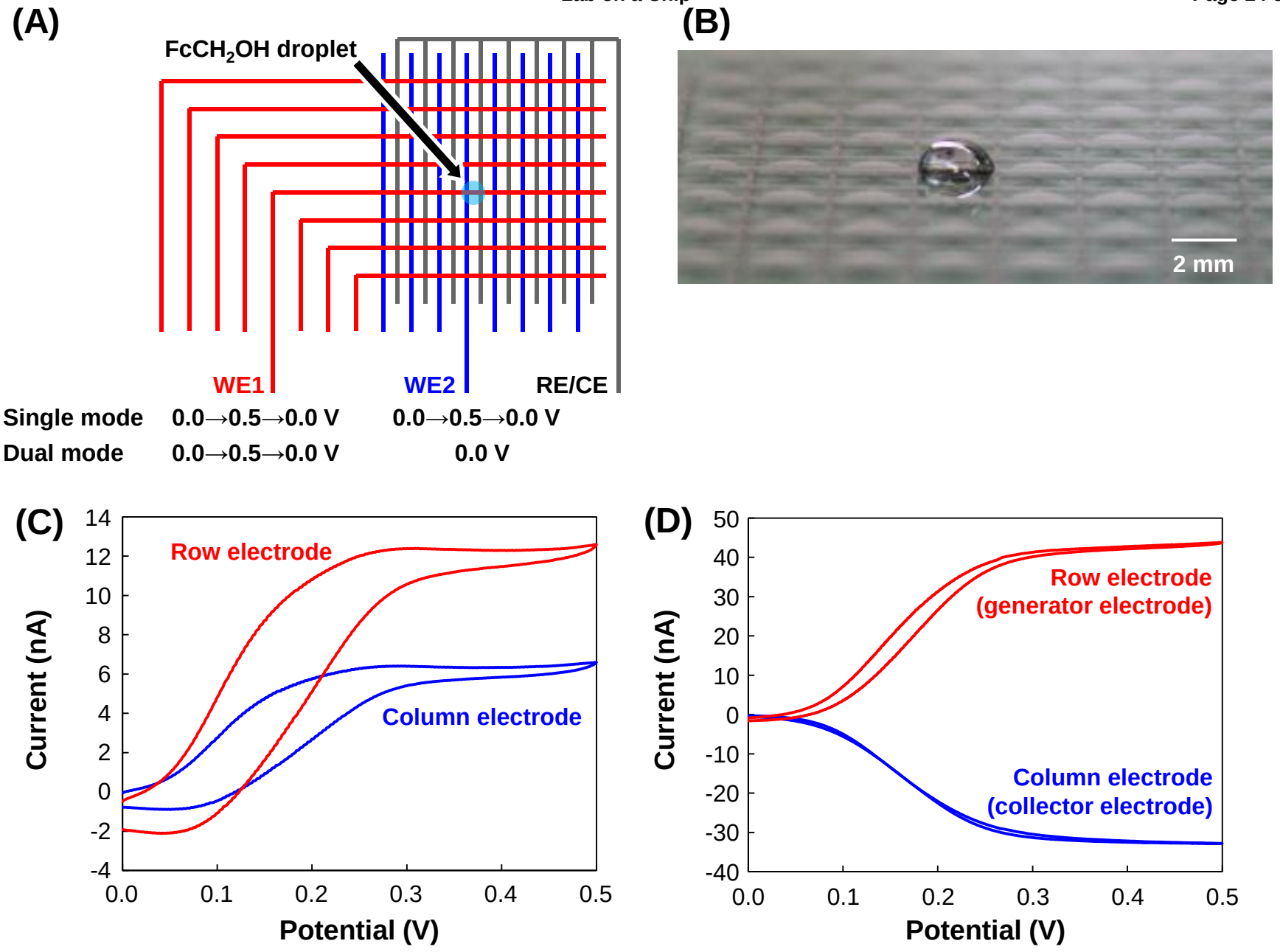

Figure 7

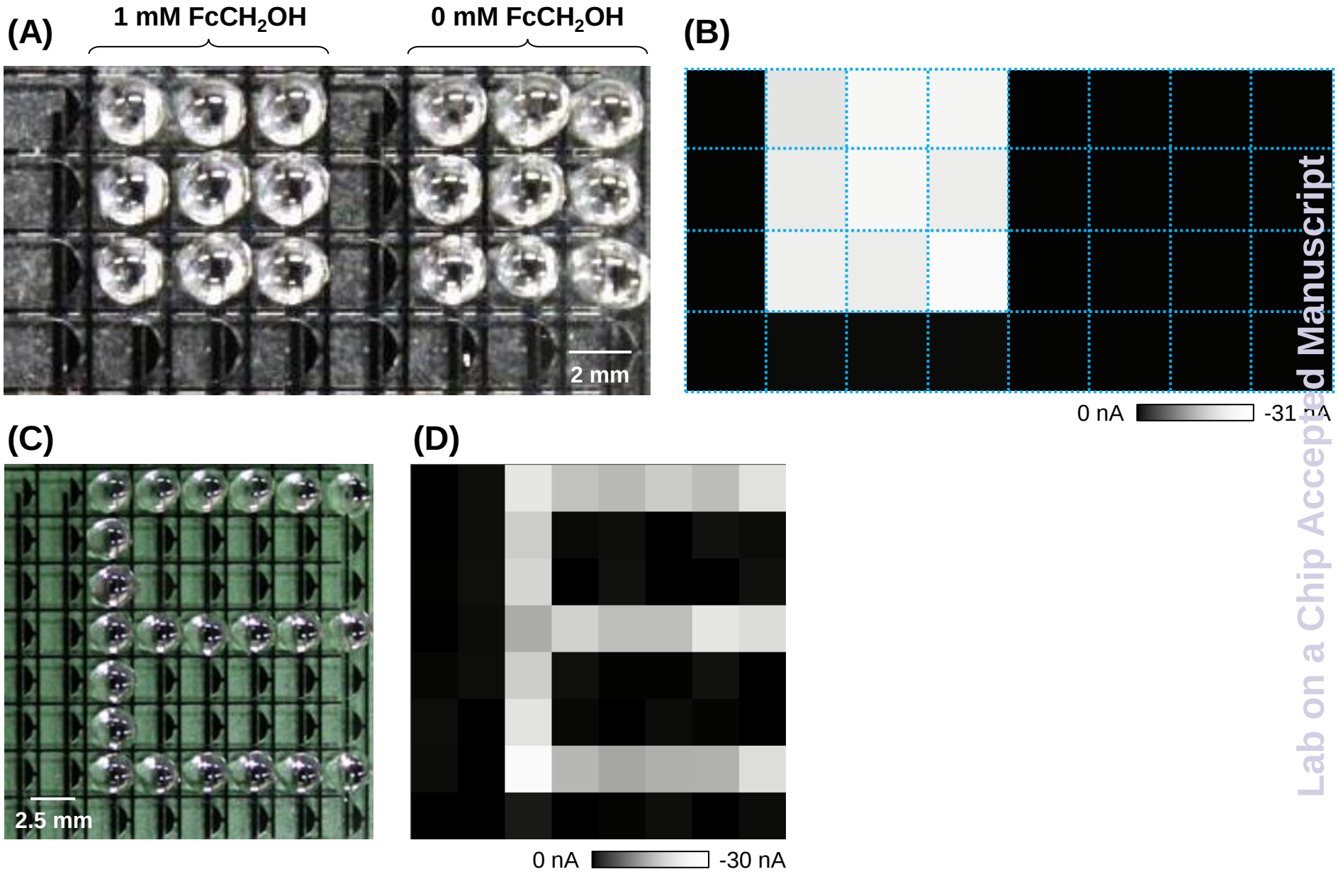

Figure 8

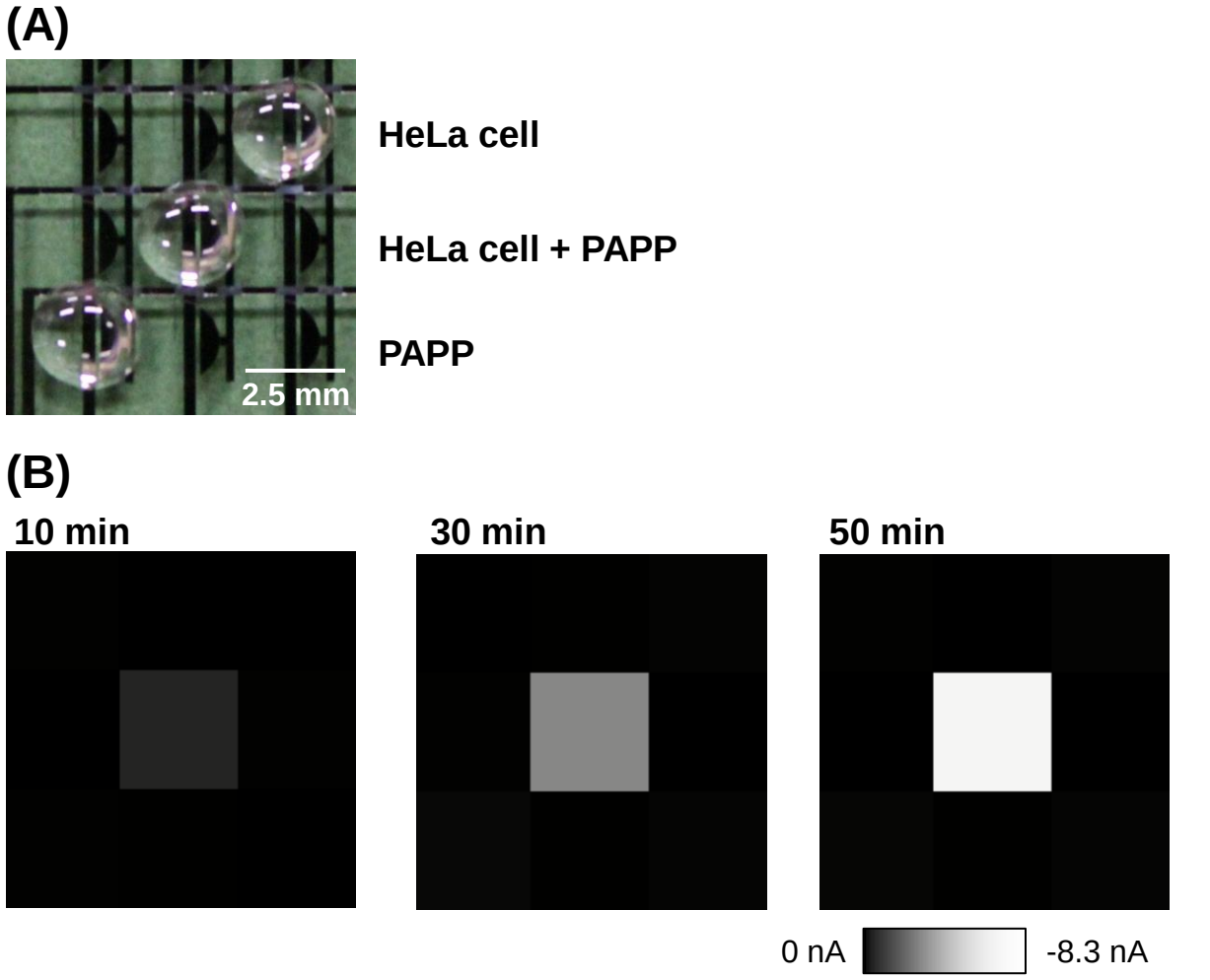

Figure 9